21st Australasian Fluid Mechanics Conference
Adelaide, Australia
10-13 December 2018

Testing of AGARD-B Standard Models in the DST Group Transonic Wind Tunnel

J. Dawes-Lynch[1] **and S.-K. Lee**[2]

[1]QinetiQ, Melbourne, VIC 3205 AUSTRALIA
[2]Defence Science and Technology Group, Melbourne, VIC 3207 AUSTRALIA

Abstract

This paper describes force and moment measurements of AGARD-B standard models in the Defence Science and Technology (DST) Group Transonic Wind Tunnel (TWT). Measurements of the lift, drag and pitching moment coefficients at Mach numbers of 0.6, 0.8 and 1.0 are compared with published data from other transonic facilities. The agreement is satisfactory for verifying the performance of the measurement system, however, small differences in the lift and moment slopes point to possible wall interference. Differences in the pitching moment characteristics of two AGARD-B models of different overall size demonstrates the integrated effects of wall interference on the data. Another key observation in the results is a step change in the AGARD-B lift curve as the angle of attack is increased from 12.5° to 14° for Mach numbers of 0.7 to 0.9, where flow hysteresis is detected at Mach number 0.9.

Introduction

The Defence Science and Technology (DST) Group Transonic Wind Tunnel (TWT) is a unique facility in Australia that is capable of producing continuous flows up to Mach number 1.4. To achieve good quality transonic flows, the test section requires ventilation into a surrounding plenum chamber via longitudinal slots and a throttled plenum evacuation system (PES). This configuration is designed to facilitate divergence of the streamlines around a test article to prevent choking of the flow, thereby increasing the maximum achievable Mach number [1]. However, the slotted test section does not adequately mitigate the effects of shock driven wall interference [2], which becomes increasingly important for testing in the transonic range. Moreover, PES suction rate can affect the streamwise pressure distribution in the test section, which may induce buoyancy errors on integrated force measurements. To help establish an understanding of the influence of these effects on force and moment measurements, it is helpful to perform tests with standard calibration models and compare these to established benchmarks, which is the aim of the present research activity.

This paper presents a selection of results from two tests conducted in the DST Group TWT using AGARD-B standard models of 75 and 100 mm diameter (D). The AGARD-B geometry was developed by the Advisory Group for Aerospace Research and Development (AGARD) as a standard model for the calibration and co-verification of transonic and supersonic wind tunnels [3]. The aerodynamic characteristics of the model are widely reported and are therefore appropriate for verification studies. The D = 75 mm model was tested first to capture data suitable for comparing to other facilities. The same tests were repeated with the D = 100 mm model to check for any differences in the measurements that could indicate wall interference. The results were also analysed in more detail to better characterise nonlinearity in the AGARD-B lift curve.

DST Group Transonic Wind Tunnel

The DST Group TWT is a closed-circuit continuous flow tunnel with a Mach number range of 0.3 to 1.2 and a stagnation pressure range of 30 kPa to 200 kPa (shown Figure 1). The tunnel can also be operated in a fixed Mach 1.4 configuration by changing the nozzle section. The main tunnel circuit is driven by a two-stage axial flow compressor and the secondary PES circuit is driven by a single stage centrifugal compressor (not shown). The test section is 0.8 m × 0.8 m square with a nominal length of 2.7 m and longitudinally slotted walls (tapered) with an open area ratio of ≈ 5%. A water-cooled heat exchanger maintains the stagnation temperature to within ±2 °C and a regenerative air dryer maintains the test-section humidity to ≈1200 ppm vol. The Reynolds number for the tunnel operational envelope is 1.8 to 29 million per metre.

The control and data acquisition system consists of a programmable logic controller, a VXI front-end and a dedicated server to host the control software and store data. During each run, the system automatically acquires data at a set of preprogrammed flow conditions and model orientations.

Standard Models and Experimental Technique

The original specification of the AGARD-B model is presented in [4]. The geometry consists of an ogive cylinder and an equilateral triangle delta wing with a symmetric circular arc profile. The model and sting dimensions are given in terms of the body diameter D, where for these tests, two models were used with D = 75 and 100 mm. The test section blockage ratio for the D = 75 mm model was 0.91% at $\alpha = 0°$ and 3.89% at $\alpha = 15°$. For the D = 100 mm model, the corresponding blockage ratios were 1.21% and 5.18%. Figure 2 shows a schematic of the model attached to the force balance and sting. The moment reference centre (MRC) is coincident with the balance moment centre (BMC) for both models. The sting is mounted on a pitch and roll system to control model attitude. The pitch can be set to ± 15° and the roll can be set to ± 180°. The sting column is translated vertically in coordination with the pitch motion so that the MRC stays on the centreline of the test section.

Forces and moments are measured using a six component strain gauge force balance. To verify the system readout, loads were applied to the balance before the model was installed using a set of calibration weights. The angular deflections of the sting and balance were also measured as a function of the applied loads as a means to correct model attitude measurements. The load ranges and standard errors for the balance are listed in

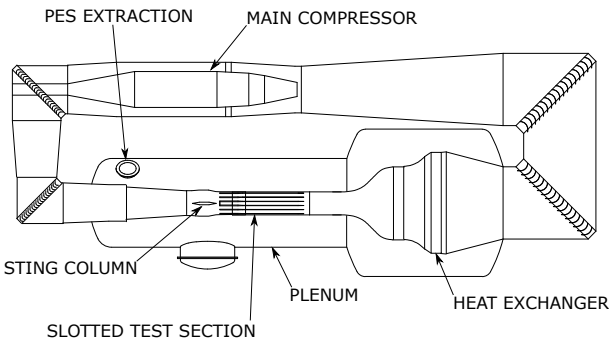

Figure 1. The DST Transonic Wind Tunnel.

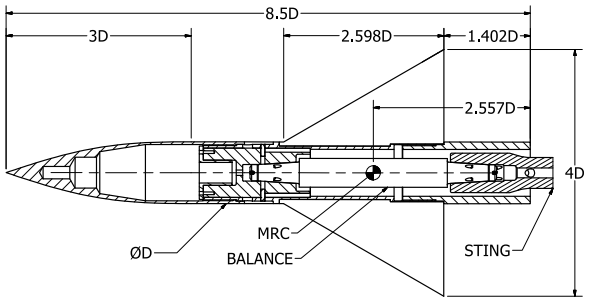

Figure 2. The AGARD-B model with sting support. The sting is joined to the balance inside the base section of the model.

Table 1. Design load ranges and standard errors for the strain gauge force balance.

Component	Design Load Range	Standard Error
Fx Drag	± 350 N	1.61 N
Fy Side Force	± 1200 N	2.19 N
Fz Normal Force	± 2500 N	2.18 N
Mx Roll Moment	± 30 Nm	0.20 Nm
My Pitch Moment	± 200 Nm	0.13 Nm
Mz Yaw Moment	± 150 Nm	0.11 Nm

Table 1. The strain-gauge signals from the force balance are digitized with a VT1413C 16 bit A/D converter and low-pass filtered at 7 Hz. Each measurement point is an average of 25 samples acquired at 10 Hz from the VXI front-end.

The free-stream Mach number, dynamic pressure and Reynolds number are calculated from measurements of the tunnel stagnation and static pressures via two Digiquartz 1030A-10 absolute pressure transducers.The tunnel stagnation pressure is the absolute pressure in the settling chamber and the tunnel static pressure is the absolute pressure in the plenum chamber. A ± 5 psid electronic scanning pressure (ESP) module is used in conjunction with a PSI8400 system to measure the base pressure of the model at two locations 180 ° apart via two tubes that are routed through the sting. A stable reference pressure for the ESP is generated by modulating a 100 psi instrument air supply against a vacuum pump, via a Proportion-Air electronic pressure regulator. The reference pressure is measured using a third Digiquartz 1030A-10 absolute pressure transducer.

In-house developed codes are employed for the reduction and analysis of TWT raw data in accordance with [5, 6]. Bias and precision uncertainties are propagated through the data reduction equations using an Automatic Differentiation (AD) algorithm, similar to that described in [7].

Results

Inter-Facility Comparisons

In this section, AGARD-B measurements from DST Group are compared with those from Arnold Engineering Development Complex (AEDC, United States) [8], the Military Technical Institute (VTI, Serbia) [9], the Institute for Aerospace Research (IAR/NAE, Canada) [9] and the Council for Scientific and Industrial Research (CSIR, South Africa) [10].

Figure 3 shows lift (C_L) as a function of α for M_∞ = 0.6, 0.8 and 1.0, where the DST Group data is taken from the tests with the D = 75 mm model. The results show good agreement with NAE and VTI, especially at M_∞ = 1.0, whereas some small differences are observed when comparing the results with AEDC and CSIR. Both of these tunnels show slightly larger average

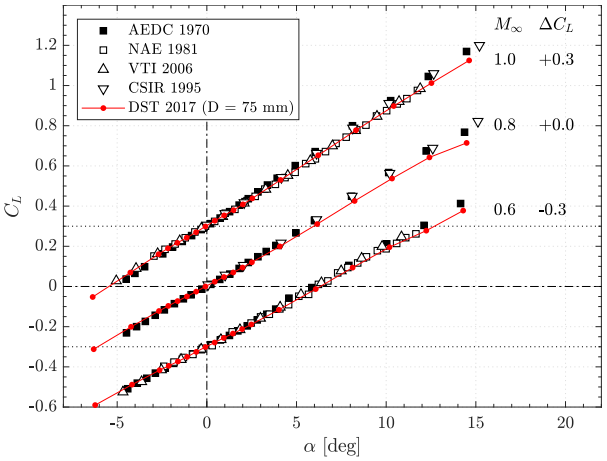

Figure 3. Lift (C_L) as a function of α. The curves for $M_\infty = 0.6$ and 1.0 are offset by -0.3 and 0.3 respectively.

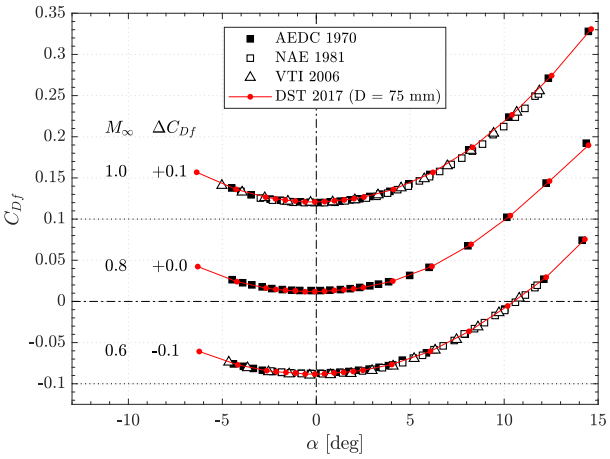

Figure 4. Fore-body drag (C_{Df}) as a function of α. The curves for M_∞ = 0.6 and 1.0 are offset by -0.1 and 0.1 respectively.

lift gradients $\partial C_L/\partial\alpha$ for each Mach number considered. Also, a nonlinearity is observed in the lift curve at M_∞ = 0.8 for $12^\circ \leq \alpha \leq 14^\circ$ that is not seen in the AEDC or CSIR results at the same condition. While these differences appear to be small, they are larger than what can be attributed to the instrumentation component of experimental uncertainty.

Figure 4 shows fore-body drag C_{Df} as a function of α. Comparison with AEDC shows that the agreement is better than for C_L, indicating that the discrepancy for $\partial C_L/\partial\alpha$ is independent of the parameters affecting drag.

Figure 5 shows pitching moment as a function of α. No data from CSIR is presented for comparison here, since the corresponding data from [10] is represented differently to the present study. The AEDC pitching moment data was modified before plotting so that the MRC was consistent for the comparison. The results agree best with VTI and NAE, whereas the average pitching moment gradient $\partial C_m/\partial\alpha$ is higher in the AEDC tunnel, similar to the lift.

Overall, the results of the force and moment tests using the D = 75 mm AGARD-B model show satisfactory agreement with the literature. The small systematic differences from AEDC and CSIR suggest that interference effects may be present in some form, however it is not possible to attribute these effects to any one facility and they are generally small enough to neglect for

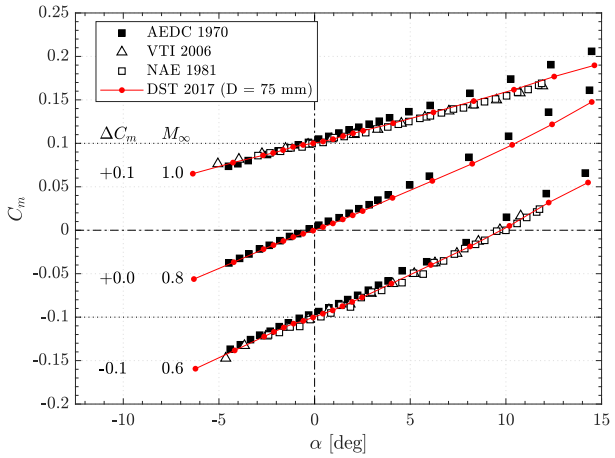

Figure 5. Pitching moment (C_m) as a function of α. The curves for $M_\infty = 0.6$ and 1.0 are offset by -0.1 and 0.1 respectively.

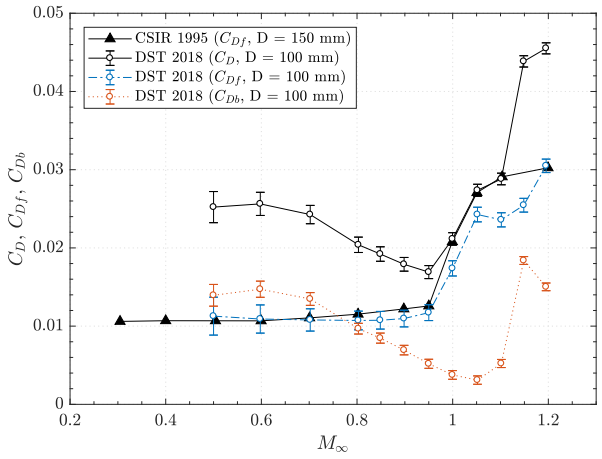

Figure 6. Drag (C_D), Fore-body drag (C_{Df}) and base drag (C_{Db}) as a function of M_∞ for $\alpha = 0°$.

the purposes of measurement system verification.

Zero Lift Drag

Figure 6 shows zero lift drag as a function of M_∞ where the DST Group data is taken from the second set of tests with the larger model (D = 100 mm). Error bars indicating the bias limits due to the instrumentation are overlaid on the data points to add context to the following analyses. Here, the uncertainty is more prominent than when considering drag as a function of angle of attack (as in Figure 4), since the variation in drag is a lot smaller. Also, the bias uncertainty decreases as M_∞ increases, since the measured forces increase.

The total drag coefficient C_D decreases as M_∞ is increased from 0.6 to the point of drag divergence at $M_\infty \simeq 0.95$. The decrease in C_D is correlated with a decrease in the base drag (C_{Db}), which is calculated from the model base pressure measurements assuming that the pressure is constant over the model base area. The difference between C_D and C_{Db} yields the forebody drag (C_{Df}) for the zero lift condition, which is nearly constant for $0.5 \leq M_\infty \leq 0.95$, suggesting that the decrease in the total drag coefficient for these conditions is due exclusively to the decrease in base drag.

The present forebody drag results agree with CSIR for $M_\infty \leq 0.95$ and show some differences for $M_\infty > 1.0$. A decrease in

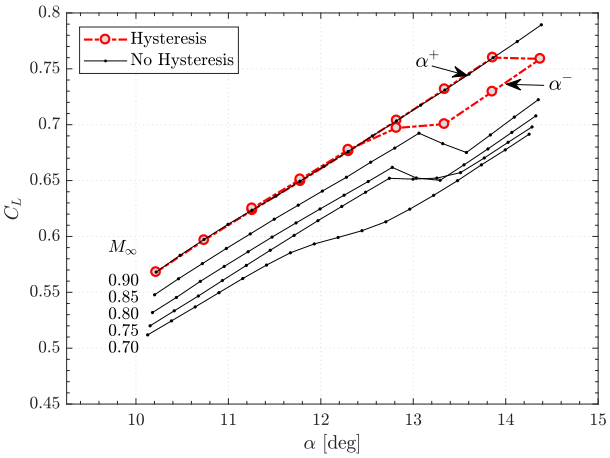

Figure 7. Lift (C_L) as a function of α for $0.7 \leq M_\infty \leq 0.9$ showing a step change in the range $12.5° \leq \alpha \leq 14°$, with hysteresis at $M_\infty = 0.9$.

C_{Df} between $M_\infty = 1.05$ and 1.10 is observed in the DST Group results, whereas for CSIR, C_{Df} increases monotonically. The decrease is correlated with a turning point in the base drag at $M_\infty = 1.05$, suggesting that the cause is associated with the flow in the base region.

Lift Curve Inflection

Additional data was acquired with the D = 100 mm model at a higher resolution of Mach number and angle of attack to investigate the nonlinearity in the C_L-α curve observed with the smaller model (as in Figure 3). Figure 7 shows C_L as a function of α for $0.7 \leq M_\infty \leq 0.9$. In these tests, the angle of attack was first varied nominally from 10° up to 14° and back to 10° in steps of 0.5° while holding the Mach number constant at each indicated value. The tests were then repeated using steps of 0.25° (in both tests, the model was held stationary as data was acquired). As Figure 7 shows, a smooth inflection is observed in the lift curve at $M_\infty = 0.7$ that evolves into a step change at higher α when M_∞ is increased. This behaviour is consistent with the numerical study of [11], where it was found that bursting of the delta wing leading edge vortex at $M_\infty = 0.8$ causes a loss of lift.

For the tests with the smaller increments in α (0.25°), the step disappeared at $M_\infty = 0.9$, as shown by the solid black line. For the tests with 0.5° steps in α, the lift behaved differently at $M_\infty = 0.9$, as shown by the red dashed curve in Figure 7. Here, as the angle of attack was increased, a step change was measured between α = 13.8° and 14.3°, whereas when the angle of attack was decreased, the step change occurred lower, between α = 12.8° and 13.4°. The lift therefore traced out a lower path over $12.8° \leq \alpha \leq 14.3°$ as α was decreased, showing that the vortex bursting exhibits hysteresis at $M_\infty = 0.9$, sensitive to the rate of change α.

Comparison of Small and Large Models

The results obtained with the larger (D = 100 mm) model were mostly similar to the smaller (D = 75 mm) model. However, differences were observed in the pitching moment curves for $M_\infty \geq 0.9$, as shown in Figure 8, where the C_m-α curves are compared at $M_\infty = 0.9$, 1.1 and 1.2. For $M_\infty = 0.9$, differences are most prevalent for $-3° \leq \alpha \leq 3°$. Here, the smaller model data shows an inflection point at α = 0°, where the sign of curvature changes from negative to positive as α is increased, whereas the larger model data is more linear. For $M_\infty = 1.1$, both curves are linear over $-2.5° \leq \alpha \leq 2.5°$, but the gradient

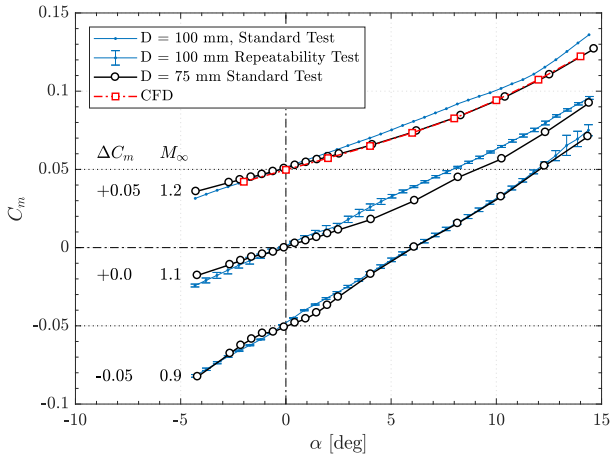

Figure 8. Pitching moment (C_m) as a function of α showing a repeatable discrepancy in the results obtained with the larger model (D = 100 mm) during the second phase of testing. The curves for $M_\infty = 0.9$ and 1.2 are offset by -0.05, and 0.05 respectively.

$\partial C_m/\partial\alpha$ is larger for the D = 100 mm model. Also at M_∞ = 1.1, the large model curve diverges from the small model curve at α = 2.5° and remains substantially higher, up to α = 14° where the results show closer agreement. The results are similar for M_∞ = 1.2, however the large model curve also diverges from the small model curve at α = 12° and the discrepancy in the measurements is significant at α = 14.5°.

The M_∞ = 0.9 and 1.1 tests with the D = 100 mm model were repeated 10 times to estimate the precision limits at each point, which are shown as error bars on the curves in Figure 8. The precision limits are indicative only of those contributions to the random uncertainty that were exercised by repeating the tests. Since the model was not removed and re-installed each time the test was repeated, the effects of model and balance misalignment are neglected. For M_∞ = 0.9, the precision limits are larger for $13.5 \leq \alpha \leq 14.5$ due to hysteresis in the pitching moment measurements that was correlated with the effects previously discussed for lift. Since all instrumentation was the same for both tests (with each model), the precision limits are a good indication of the experimental uncertainty for the comparison. Moreover, since the discrepancies identified in the pitching moment curves are generally greater in magnitude than the precision limits, they are repeatable and therefore cannot be attributed to random errors.

Figure 8 also includes results from a Reynolds Averaged Navier-Stokes (RANS) computational fluid dynamics (CFD) simulation of the AGARD-B model in a freestream flow at M_∞ = 1.2 (taken from [13]). At this condition, the CFD pitching moment predictions show excellent agreement with the smaller model measurements. This result suggests that it is more likely that the larger model was affected by wall interference.

Concluding Remarks

Verification testing plays an important role in transonic wind tunnel operations. The AGARD-B standard model is often used for this purpose, since its aerodynamic characteristics are well reported in the literature. In this paper, results from AGARD-B tests in the DST Group TWT are described. Lift, drag and pitching moments were measured in these tests, for Mach numbers in the range 0.6 to 1.2 at angles of attack in the range -14° to 14°. The results generally compare favourably to other facilities, however small differences in the lift and pitching moment curve gradients, possibly due to minor wall interference effects, are noted. When the force and moment tests were repeated with a 33% larger AGARD-B model, the lift and drag results were very similar, however clear differences emerge in the pitching moment measurements at Mach numbers greater than 0.9, suggesting that the results in either case are affected by wall interference. By comparing these results with a RANS simulation of the freestream case, it was predicted that these effects were most prominent for the larger model.

To extend on the comparative analysis, a nonlinearity in the AGARD-B lift curve for Mach numbers in the range 0.7 to 0.9 was also investigated, where hysteresis in the lift curve was detected at Mach number 0.9.

Acknowledgements

Thanks go to P. O'Connor, A. Monks, B. Lemke, S. Lam, A. Snowden, B. Loxton and P. Hayes for their contributions.

References

[1] Wright, R. H., Ward, V., G., NACA Transonic Wind-Tunnel Test Sections, National Advisory Committee for Aeronautics, Report 1231, 1955.

[2] Goethert, B. H., Physical Aspecs of Three-Dimensional Wave Reflections in Transonic Wind Tunnels at Mach Number 1.20 (Perforated, Slotted, and Combined Slotted-Perforated Walls, Propulsion Wind Tunnel Facility, Arnold Engineering Development Center, Air Research and Development Command, AEDC-TR-55-45, 1956.

[3] A Review of Measurements on AGARD Calibration Models, The Advisory Group for Aerospace Research and Development, AGARDograph 64, 1961.

[4] Specifications for AGARD Wind Tunnel Calibration Models, AGARD Memorandum AG-4/M3, 1955.

[5] Farlie, B., Algorithms for the Reduction of Wind-Tunnel Data Derived from Strain Gauge Force Balances, Defence Science and Technology, DSTO-TR-0899, 1999.

[6] Assessment of Experimental Uncertainty with Application to Wind Tunnel Testing, American Institute of Aeronautics and Astronautics, AIAA Standard S-071A-1999.

[7] Hall, B. D., Calculating Measurement Uncertainty using Automatic Differentiation, Meas. Sci. Technol., **13** (421), 2002, 421–427

[8] Anderson, C. F., An Investigation of the Aerodynamic Characteristics of the AGARD Model B for Mach Numbers from 0.2 to 1.0, Propulsion Wind Tunnel Facility, Arnold Engineering Development Center, Air Force Systems Command, AEDC-TR-70-100, 1970.

[9] Damljanovic, D., Vitic, A. and Vukovic, D., Testing of AGARD-B Calibration Model in the T-38 Trisonic Wind Tunnel, Scientific Technical Review, **56** (2), 2006, 52–56.

[10] Lombardi, G. and Morelli, M., Analysis of some Interference Effects in a Transonic Wind Tunnel, Journal of Aircraft, **32** (3), 1995, 501–509.

[11] Tuling, S., Vallabh, B. and Morelli, M.F., Compressibility Effects for the AGARD-B Model, The Aeronautical Journal, **119** (1214), 2016, 543–552.

[13] Dawes-Lynch, J. and Snowden, A., Testing of an AGARD-B Calibration Model in a Transonic Wind Tunnel, Defence Science and Technology, DST-Group-CR-2018-0052.